Egyptian Journal of Chemistry

http://ejchem.journals.ekb.eg/

In Vitro Anticancer and Antibacterial Assessment of Novel Metal Complexes of 1,3-di-[P-Tolyl]-2,4-di-[9H-Purin-6-Yl]-2,4-Dichlorocyclodiphosph(V)Azane

Asmaa A. Hamed [1*], Carmen M. Sharaby [1], Mona F. Amine [1], Youssry A. Ammar [2] and Ahmed A. El-Sherif [3]

[1] *Chemistry Department, Faculty of Science, Al-Azhar University (Girls), Nasr City, Cairo, Egypt*

[2] *Chemistry Department, Faculty of Science, Al-Azhar University (Boys), Nasr City, Cairo, Egypt*

[3] *Chemistry Department, Faculty of Science, Cairo University, Giza, Egypt*

Abstract

ron, copper, zinc, cadmium, and silver complexes of 1,3-di-[p-tolyl]-2,4-di-[9H-purin-6-yl]-2,4-dichlorocyclodiphosph(V)azane, H2L ligand were performed and characterized using spectroscopic and analytical techniques. The 1:2(L:M) complex structures of such complexes were revealed by spectroscopic analysis. The spectroscopic findings also suggested an octahedral structure for all complexes except for the tetrahedral silver complex. The ligand was coordinated to metal ions through exocyclic-NH and pyrimidine-N. Furthermore, computational studies of the H2L ligand were performed by the DFT/B3LYP methodology in which the ligand was improved. HOMO and LUMO energy values, chemical hardness, electronegativity, softness, and other parameters were calculated. The antitumor activity of all produced compounds was studied versus, human being breast carcinoma and human being colorectal carcinoma cell lines (MCF-7 & HCT-116). Additionally, antibacterial, and antifungal activity were also investigated.

Keywords: Nucleobase, cyclodiphosph(V)azane derivative, metal complexes, molecular modeling, antimicrobial, anticancer activity.

1. Introduction

Over the last few decades, there has been tremendous interest in cyclophosph(V)zanes due to their extensive chemical and structure flexibility[1]. The four-membered P2N2 heterocycles have received special attention in light of their remarkable capability to act as adaptable building blocks in the design and assembly of an extensive variety of great inorganic bases[2], fire retardant[3], potential carcinostatics among other pharmacological activities [4] and their ability as multidentate ligands [5]. Cyclophospha(V)zane is a strong and efficient flame retardant. This class of compounds has been synthesized by Mingsheng Liu et.al, taking use of a cyclodiphosphazane derivative's strong reactivity. After FR treatment, cotton textiles have dramatically increased fire resistance[6]. The copper complex of cyclodiphospha(V)zane ligand showed high activity against S. aureus and cleaved DNA, making it a good drug candidate has been reported by A.M.A Alaghaz and co-workers.[7]. Nucleophilic substitution of chlorine atom(s) is the main reason for the high reactivity of hexachlorocyclodiphospha(V)zane[8]. Transition metals are a significant class of compounds because they are related to a wide range of biological functions[9]. Coordination chemistry helps researchers to understand biological processes and get new medications[9]. Pyrimidine and purine-containing compounds are found in nucleic acids, many vitamins, coenzymes, and antibiotics, among other biological systems[10]. Nucleobases are considered useful ligands for metal binding[11], due to their interest in structural, thermodynamic, and kinetic research related to biology and chemistry[12]. In dispersions and emulsions, particle size reduction with ultrasound is a tried-and-true technique. Because of the potential for deagglomeration and reduction of

*Corresponding author: Asmaaahmed152@Azhar.edu.eg (Asmaa Hamed); ORCID 0000-0003-4162-3928

Receive Date: 23 August 2022, **Revise Date:** 16 October 2022, **Accept Date:** 31 October 2022,

First Publish Date: 31 October 2022

DOI: 10.21608/EJCHEM.2022.158055.6840

primary, ultrasonic processors are utilized to create slurries and emulsions of nanoscale materials[13].

In this article, substituted nucleobase-cyclodiphosph(V)azane derivative (H_2L) has been synthesized as described in the literature,[8] and its activity experimented towards some transition metal ions. Classification of reconstituted mixtures was conducted using different physicochemical methods. Antimicrobial and antitumor activities for prepared ligand and the complexes of it was examined.

2. Experimental

1.1. Materials and reagents

Chemical substances utilized were of the analytical reagent class (AR), and supreme purification level. PCl_5, para-toluidine, adenine (9H-purin-6-amine), ferric chloride hexahydrate ($FeC1_3.6H_2O$), ferrous sulphate heptahydrate ($FeSO_4.7H_2O$), zinc chloride anhydrous ($ZnC1_2$), copper chloride dihydrate ($CuC1_2.2H_2O$), cadmium chloride dihydrate ($CdC1_2.2H_2O$) and silver nitrate ($AgNO_3$) were purchased from Merck or Sigma where, the organic solvents ethanol, diethylether, deuterated dimethylsulfoxide (DMSO), and dimethylformamide (DMF), were purchased from BDH. Perchloric acid, ammonium chloride, ammonia solution, nitric acid, and ethylenediaminetetraacetic acid disodium salt (EDTA) were Merck products. Also, Murexide, salicylic acid, Eriochrome black-T (E.B.T), and p-chloroaniline which were used as indicators were Merck goods. All preparations were conducted in de-ionized water.

1.2. Instrumentation

At Cairo University's Micro Analytical Center, C, H, N, Cl, and S microanalysis measurements were made. Following complete breakdown of the complexes, the metal contents were evaluated by titration against a standard EDTA solution, and the phosphorus contents were quantified gravimetrically[14]. Using a direct insertion probe (DIP) and a Shimadzu-Ge-Ms-QP 100-EX mass spectrometer (Japan), mass spectra were logged between 50 and 800 °C. Using a Perkin-Elmer Lambda 3B UV-vis spectrophotometer, the UV-vis spectra were captured. The IR spectra were documented on a PerkinElmer 437 IR spectroscopy (400-4000cm^{-1}) (KBr technique). TMS was used as an internal standard and ^1H, Using a Burker FT-400 MHZ spectroscopy, ^{13}C NMR spectra of DMSO-*d6* were evaluated. SEM Model Quanta 250 FEG (Field Emission Gun) with EDX unit (Energy Dispersive X-ray Analyses), with accelerating voltage 30 K.V., magnification 14X up to one million, and resolution for Gun.1n, Desert Research Center, Egypt, was used to create the SEM picture of the complexes. Complexes' magnetic susceptibilities were measured using a Sherwood Scientific Magnetic Susceptibility Stability. ESR spectra for copper complex in solid state at room temperature were recorded by Klystron - X-band (has frequency 9.5 Giga Hertz and wavelength is about 3cm.) EMX spectrometer (Germany) using a standard rectangular cavity of ER 4102 with appropriate microwave power (5–10mW) and 100 kHz magnetic field modulation. Waveguide to transfer the microwave radiation from klystron to the sample. 5-Quartz tubes that have an inner diameter of about 3 or 5 mm are generally used to contain solid or solution samples[15]. DPPH was used as a standard material.

A Shimadzu TGA-50H was used for the thermogravimetric analysis, and a flow rate of 20 ml min^{-1} was used. Geometry optimization was done utilizing DFT simulations to gain structural data about the produced nucleobase-cyclodi-phospha(V)zane derivative. The B3LYP technique was used to perform the calculations[16].

Using DMF as a solvent, the antimicrobial activity was conducted. The test was done using the broth dilution method[16]. The antitumor activity was performed against (MCF-7) and (HCT-116) carcinoma cell lines.

1.3. Synthesis of cyclodiphosph(V)azane ligand (H_2L)

9H-purin-6-amine (2.7g, 0.02 mole) in 100ml acetonitrile was combined -in little portion- to a highly stirred and low temp. solution of 2,2,2,4,4,4-hexachloro-1,3-di-p-tolyl-cyclodiphosphazane (4.85 g, 0.01mol) in 100ml acetonitrile in the quick fit flask during half an hour, has been described in the literature,[8]. After the addition was completed, the reaction blend was left under reflux for about three hours, Separation of the solid output produced has been done by filtering then purified by washing several times with acetonitrile, diethyl ether, and then dried under vacuum over anhydrous $CaCl_2$ to give corresponding substituted cyclodiphosphazane, H_2L ligand. Yield 80%; white solid, m.p = 265°C. Anal. Calcd. For $C_{24}H_{22}Cl_4N_{12}P_2$ (682.27) (%): C, 42.25; H, 3.25; N, 24.64; Cl, 20.78; P, 9.08. Found (%): C, 41.97; H, 3.06; N, 24.64; Cl, 20.22; P, 8.87. IR (υ, Cm^{-1}): 3260sharp (NH); 1699sharp (C=N) imidazole; 1170medium (P-N) and 605sharp (P-Cl). UV-vis. (DMF) (λ_{max}, nm): 277 (phosph(V)azo four-membered ring) and 310(π-π*). ^1H NMR (500 MHz, DMSO-d_6): 9.18ppm (br., 2H, NH); 8.54,8.49ppm (s, 2H, C-H heterocycle); 6.91-7.27ppm (4, 4H, Ar. protons) and 2.31ppm (s, 3H, CH_3). ^{13}C NMR (500 MHz, DMSO-d_6): δ=20.9(C_1); δ=115.9 (C_2); δ=121.8 (C_3); δ=130.4 (C_4); δ=132.1 (C_5); δ=137.8 (C_6); δ=143.0, 147.7 ($C_{7,8}$); δ=150.0 (C_9); δ=152.9 (C_{10}).

1.4. Synthesis of metal complexes

A heated ethanolic solution of H_2L (5 mmol) was added dropwise to a somewhat high-temperature ethanolic solution containing Fe(III), Fe(II), Cu(II), Zn(II), Cd(II), and Ag(I) metal salts (10 mmol). Reaction blend was refluxed for 2h. The formed

precipitate in each case was gathered by purification, washed with ethanol and diethyl ether, and then dried up in vacuum.

$[(FeCl_3)_2(H_2L)(H_2O)_2]$ (1), Yield, 16%, pale yellow solid, m.p >300ºC. Anal. Calcd. % for $C_{24}H_{26}Cl_{10}Fe_2N_{12}O_2P_2$ (M.wt, 1042.69) : C, 27.65; H, 2.51; N, 16.12; Cl, 34.00; P, 5.94; Fe, 10.71. Found: C, 27.33; H, 2.08; N, 15.75; Cl, 33.68; P, 5.61; Fe, 10.36. IR (υ, cm^{-1}): 3228broad (NH); 1690sharp (C=N) imidazole; 1180medium (P-N); 640medium (P-Cl); 893medium (Coord. H_2O); 529 (M–O); 468 (M–N). μeff (BM): 6.1. *Λ*m (Ω−1 mol−1 cm2): 3.06.

$[(FeSO_4)_2(H_2L)(H_2O)_4]$ (2), Yield, 42%, Off white solid, m.p >300ºC. Anal. Calcd. % for $C_{24}H_{29}Cl_4Fe_2N_{12}O_{12}P_2S_2$ (M.wt, 1057.13) : C, 27.24; H, 2.86; N, 15.88; S, 6.06; Cl, 13.40; P, 5.85; Fe, 10.56. Found%: C, 26.94; H, 2.36; N, 15.55; S, 5.81; Cl, 13.19 P, 5.48; Fe, 10.29. IR (υ, cm^{-1}): 3252broad (NH); 1691sharp (C=N) imidazole; 1146 sharp (P-N); 610medium (P-Cl); 887weak (Coord. H_2O); 531 (M–O); 450 (M–N). μeff (BM): 4 *Λ*m (Ω^{-1} mol^{-1} cm^2): 6.13.

$[(CuCl_2)_2(H_2L)(H_2O)_4]$ (3), Yield, 58%, green solid, m.p >300ºC. Anal. Calcd. % for $C_{24}H_{30}Cl_8Cu_2N_{12}O_4P_2$ (M.wt, 1023.22) : C, 28.17; H, 2.54; N, 16.43; Cl, 27.72; P, 6.05; Cu, 12.42. Found%: C, 27.74; H, 2.54; N, 16.11; Cl, 27.33; P, 5.75; Cu, 12.19. IR (υ, cm^{-1}): 3387broad (NH); 1661sharp (C=N) imidazole; 1173 sharp (P-N); 613medium (P-Cl); 876medium (Coord. H_2O); 564 (M–O); 404 (M–N). μeff (BM): 1.7. *Λ*m (Ω^{-1} mol^{-1} cm^2): 0.83.

$[(ZnCl_2)_2(H_2L)(H_2O)_4]$ (4), Yield, 20%, White solid, m.p >300ºC. Anal. Calcd. % for $C_{24}H_{30}Cl_8Zn_2N_{12}O_4P_2$ (M.wt, 1026.89) : C, 28.07; H, 2.94; N, 16.37; Cl, 27.62; P, 6.03; Zn, 12.73. Found%: C, 27.71; H, 2.51; N, 15.98; Cl, 27.21; P, 5.66; Zn, 12.39. IR (υ, cm^{-1}): 3356sharp (NH); 1690sharp (C=N) imidazole; 1115sharp (P-N); 634medium (P-Cl); 808weak (Coord. H_2O); 535 (M–O); 404 (M–N). ^1H NMR: 8.94ppm (br., 2H, NH); 8.48,8.49ppm (s, 2H, C-H heterocycle); 6.90-7.28ppm (d, 4H, Ar. protons) and 2.49ppm (s, 3H, CH_3); 3.6ppm (br., 2H, H_2O coordinated water). μeff (BM): diamagnetic. *Λ*m (Ω^{-1} mol^{-1} cm^2): 2.82.

$[(CdCl_2)_2(H_2L)(H_2O)_4]$ (5), Yield, 20%, White solid, m.p >300ºC. Anal. Calcd. % for $C_{24}H_{30}Cl_8Cd_2N_{12}O_4P_2$ (M.wt, 1120.96) : C, 25.72; H, 2.70; N, 14.99; Cl, 25.30; P, 5.53; Cd, 20.06. Found%: C, 25.34; H, 2.43; N, 14.64; Cl, 24.99; P, 4.99; Cd, 19.90. IR (υ, cm^{-1}): 3324sharp (NH); 1655sharp (C=N) imidazole; 1173weak (P-N); 678weak (P-Cl); 837medium (Coord. H_2O); 532 (M–O); 487 (M–N). ^1H NMR: 8.92ppm (br., 2H, NH); 8.48, 8.49ppm (s, 2H, C-H heterocycle); 6.92-7.28ppm (d, 4H, Ar. protons) and 2.49ppm (s, 3H, CH_3); 3.9ppm (br., 2H, H_2O coordinated water). μeff (BM): diamagnetic. *Λ*m (Ω^{-1} mol^{-1} cm^2): 2.78.

$[(AgNO_3)_2(H_2L)(H_2O)_2]$ (6), Yield, 45%, Gray solid, m.p >300ºC. Anal. Calcd. % for $C_{24}H_{24}Cl_4Ag_2N_{14}O_8P_2$ (M.wt, 1056.27) : C, 27.30; H, 2.29; N, 18.57; Cl, 20.43; P, 5.87; Ag, 20.43. Found%: C, 26.84; H, 1.95; N, 18.22; Cl, 20.18; P, 5.38; Ag, 20.05. IR (υ, cm^{-1}): 3356broad (NH); 1689sharp (C=N) imidazole; 1150medium (P-N); 602medium (P-Cl); 895medium (Coord. H_2O); 524 (M–O); 472 (M–N). ^1H NMR: 8.86ppm (br., 2H, -NH); 8.48, 8.49ppm (s, 2H, C-H heterocycle); 6.62-7.25ppm (d, 4H, Ar. protons) and 2.49ppm (s, 3H, CH_3); 3.9ppm (br., 2H, H_2O coordinated water). μeff (BM): diamagnetic. *Λ*m (Ω^{-1} mol^{-1} cm^2): 1.55.

1.5. Synthesis of nanosilver complex

Nanosilver complex was prepared from the ordinary silver complex, which was obtained, then an ethanolic solution of one gram of the resulting ordinary silver complex precipitate was stirred magnetically for 4 hrs. at 40 ºC to get nano-sized silver complex using ultrasonic conversion. The next steps were filtering the finished solid product, washing it with ethanol then drying it in vacuum along $CaCl_2$ (anhydrous.)

1.6. Biological activity

To increase the likelihood of discovering their antibiotic potential, more than one strain was employed to evaluate the antibacterial activity of the metal complexes formed from the generated H_2L ligand. The free H_2L ligand and its metal complexes were screened against *Gram-positive(+ve) bacteria*; *Bacillus pumilis (MTCC-2296)* and *Streptococcus faecalis (MTCC-0459), Gram-negative(-ve) bacteria; Escherichia coli (ATCC-25955)* and *Enterobacter cloacae (ATCC-23355), Yeast; Candida albicans (ATCC-10231)* and *fungi; Aspergillus niger (MTCC-1881)* to assess their potential antibacterial and antifungal activities. Using the broth dilution method, the antibiotics Penicillin G and Ciprofloxacin were employed as the standard antibacterial controls, while ketoconazole was utilized as the standard yeasts and fungi control[17]. Using the broth dilution technique, bacteria are injected into a liquid growth medium using various concentrations of an antimicrobial agent. Spectrophotometric cell counts are used to measure microbial growth following an established incubation period. The chemical's minimum inhibitory concentration (MIC) value is the concentration at which it stops the development of the microorganism[16]. The free ligand (H_2L) and its metal complexes were conducted *versus* carcinoma of human being breast and carcinoma of human being colorectal (MCF-7 and HCT-116 respectively) cell

lines; respectively. Doxorubicin was used as a standard human cancer drug.

2. *Results and discussion*

2.1. Ligand Synthesis and Characterization

Reaction of p-toludine with PCl_5 gives rise to the dimer, 1,3-di-[p-tolyl]2,2,2,4,4,4-hexachlorocyclo-diphosph (V)azane, (L) which was then reacted with 9H-purin-6-amine to produce the desired ligand, (H_2L) as shown in Scheme.1,2. Spectroscopic and analytical techniques were used to confirm the structure of the H_2L which agreed with that has been described in literature, [8].

Free H_2L ligand had a sharp melting point, demonstrating its purity when manufactured. The mass spectrum revealed a molecular ion peak at m/z=682(26%), supporting the ligand's reported molecular formula ($C_{24}H_{22}C_{l4}N_{12}P_2$). Also, the mass spectrum recorded the most intense ion (base peak) at m/z=458 (100%) which is compatible with the molecular formula ($C_{12}H_{13}Cl_2N_{12}P_2$). The UV–vis spectrum of the H_2L free ligand in (10^{-3}M) using DMF as a solvent Table 1 showed absorption band at 277nm characteristic for Phosphazo four-membered ring of the dimeric structure[18,19]. The IR data for H_2L ligand showed characteristic vibration bands at 1170cm^{-1} and 605cm^{-1} which are characteristic for υ(P-N) and υ(P-Cl) groups; respectively[20,21]. Also, it has two additional bands at 3260cm^{-1} and 1699cm^{-1} attributed to the υ(NH) and υ(C=N) pyrimidine ring; respectively[22]. The isolated H_2L free ligand's ^{1}H, ^{13}C NMR spectra, which were captured in DMSO-d_6 at room temperature, displayed recognizable proton signals. Exocyclic N-H and imidazole N-H singlets, which virtually overlapped, were ascribed to the observed wide signal at δ =9.18ppm (exchangeable with D_2O)[23]. Signals at δ=8.52ppm and δ=8.54ppm suggested (C-H) imidazole and pyrimidine protons[8]; respectively and the signal at δ=2.32ppm assigned to (-CH_3) protons[24,25]. Along with additional doublet doublet indications for H_2L free ligand in the range 6.91–7.27ppm ascribed to aromatic protons[26]. ^{13}C NMR spectrum of H_2L ligand shows a peak at 20.96ppm corresponding to the carbon atom of methyl group[27]. While the peak observed at 40 ppm is due DMSO-*d6*. Signals observed in range (121.89-132.91) ppm are characteristic of different aromatic carbon positions[27,28]. The measured signals at 143.00 and 147.72 ppm were attributed to the benzene carbon atoms linked to the nitrogen atoms of the phospha(V)azo ring. As indicated in Table 2, the other ^{13}C signals, on the other hand, were caused by the carbon atoms in two pyrimidine and purine rings.

2.2. Computational studies on H_2L ligand

An improved structure of H_2L free ligand has been achieved using Gaussian software at DFT level of theory[29]. The 6-31G(d,p) basis set and B3LYP functional was used for the geometry optimization using the doublet spin of the molecule Scheme.2. Table 3 lists the prepared ligand's bond lengths, bond angles, and dihedral values. In addition to, the total energy, dipole moments, quantum chemical parameters such as absolute electrophilicity index (*χ),* hardness *(η),* global electrophilicity *(ω),* chemical potential *(Pi),* absolute softness *σ,* global softness *(S),* additional electronic charge (ΔN_{max}) and energy gap (ΔE), which explain energy variance between LUMO (Lowest unoccupied molecular orbital) and HOMO (Highest occupied molecular orbital) are tabulated within Table 3.

From the results, it was found that the small energy gap value of ΔE (E_{LUMO}-E_{HOMO}) for the free (H_2L) ligand which was found to be 4.30 eV is considered a good indication to capability of complexation with neighboring central metal ion which have empty *d*-orbital[30]. Also, the negative value of chemical potential (*Pi*) was a positive sign for the prepared ligand stability, also that it does not decompose spontaneously[31]. The high value of electrophilicity index (χ) equal to 3.78 indicates that the ligand is good for docking in biological activities[32].

The total of computed internal angles in $(P–N)_2$ four membered ring is ∼360◦, therefore, the phosphazo four-membered ring is planar. In addition, the benzene ring makes 89.2° and 90.5° dihedral angle with the phosphazo ring which indicates that the benzene ring is perpendicular to the phosphazo ring, while the nucleobase ring makes 179.9° dihedral angle with the phosphazo ring which indicates that the nucleobase ring in the same plane of the phosphazo ring. The four-membered ring strain, on the other hand, has given the phosphorus atom a deformed trigonal bipyramidal geometry. Nitrogen atoms (N_5 and N_{62}) of exocyclic N – H are slightly triagonal pyramidal with a dihedral angle ∼ 180◦ of (P_4 – N_5 – H – C_{32}, P_2 – N_{62} – H – C_{29}) [8] (Table 3, Scheme.2.)

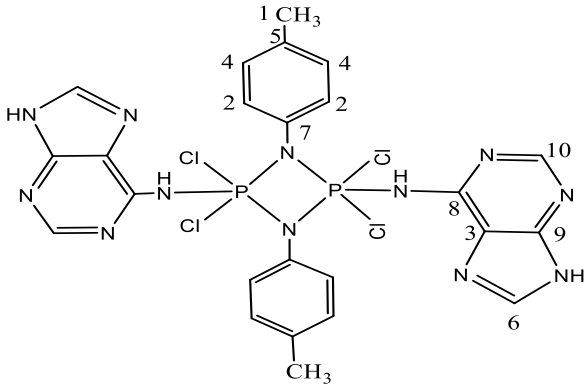

Scheme.1. suggested structure of synthesized H_2L free ligand

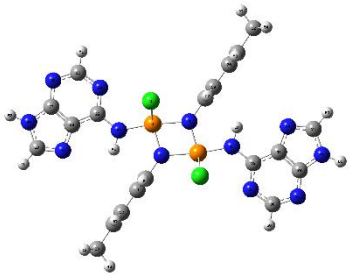

Scheme.2. The optimized structure of H_2L free Ligand

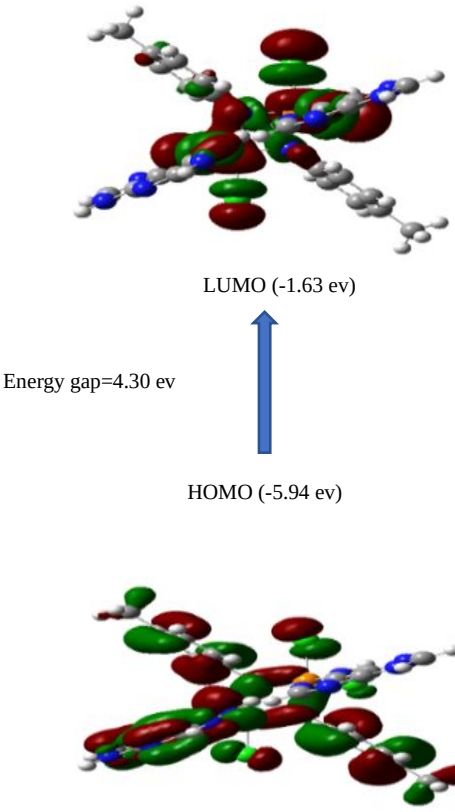

Fig.1. HOMO and LUMO molecular orbital

2.3. Composition and structure of metal complexes

Elemental analysis (C, H, N, Cl, S and P), UV-vis, FT-IR, 1H NMR, X-ray, molar conductance, magnetic studies, and thermal investigations were used to clarify the metal complexes of the H_2L ligand, Fe(III), Fe(II), Cu(II), Zn(II), Cd(II), and Ag(I) ions (TGA). The data shows that the results of elemental analysis match those of the proposed structures Fig.2. Insoluble in water, the complexes are soluble in DMSO and DMF solvents.

The values of molar conductance in dimethylformamide (DMF) of the metal complex solutions 10^{-4}M were found in the range 0.83-6.13 $\Omega^{-1}cm^2$ mol^{-1}. The generated complexes are not electrolytes, as evidenced by the low molar conductance values[24,30]. This is consistent with the conductivity readings being below 50 Ω^{-1} mol^{-1} cm^2 for a nonelectrolyte in DMF solution.

From their mass spectrum data, more information on the hypothesized structures of examined metal complexes was obtained. The possible fragmentation pathway of Zn(II), Cd(II) and Ag(I) complexes showed existence of peaks at m/z=987(22%), 992(17%) and 996(20%) which agree to molecular formula ($C_{24}H_{24}Cl_8N_{12}O_2P_2Zn_2$, $C_{24}H_{30}Cl_4$ $N_{12}O_4P_2Cd_2$ and $C_{22}H_{18}Cl_4N_{14}O_6$ P_2Ag_2) for Zn(II), Cd(II) and Ag(I) complexes, respectively. Mass spectra also show a base peak at m/z= 427(100%), 53(100%) and 360(100%) for Zn(II), Cd(II) and Ag(I) complexes, respectively. In addition, mass spectral data showed other proposed fragments with good intensity which confirm the stability of these fragments.

Table 1 displays the electronic spectra for the metal complexes visible in ($l0^{-3}$M) DMF at room temperature, with wavelengths ranging from 200 to 800 nm. Electronic spectra of newly prepared metal complexes showed a sharp and intense band in the region 268-274nm, corresponding to phospazo four-membered ring[4,28]. Nevertheless, depending on the kind of metal ion present and the complexation process, the absorptions were moved to lower wavelengths with regard to the ligand. The spectra of complexes showed absorption bands in the range 300-326nm due to $\pi\rightarrow\pi^*$ and the range absorption bands at 328-369nm are due to $n\rightarrow\pi^*$ transitions[33,34], credited to the presence of electronegative atoms. A band in the complexes' spectra that can be attributed to the ligand-to-metal (L-MCT) transition can also be seen between 387 and 430 nm [4,24]. For Fe(III) complex a *d-d* transition observed at 560nm (17,857cm^{-1}) due to $^6A_{1g}\rightarrow{}^5T_{1g}$ transition in octahedral geometry[4,35,36]. The observed magnetic moment value 6.1 B.M. confirm octahedral geometry for Fe(III) complex[26,35]. While Fe(II) displayed absorption bands at 528, 663 and 735nm (18,939, 15,082 and 13,605cm^{-1}) which are assigned to $^5T_{2g}\rightarrow{}^5E_g$ transition[24,35]. The observed magnetic moment 4 B.M. is consistent with an octahedral geometry[35]. Copper(II) complex gave two main bands at 573 and 667nm (17,452 and 14,992cm^{-1}) due to $^2E_g\rightarrow{}^2T_{2g}(x^2–y^2)$ transition[24]. The measured magnetic value was found as 1.7 B.M. which suggested an octahedral environment for copper complex[37]. In contrast to Fe(III), Fe(II), and Cu(II) complexes, Zn(II), Cd(II), and Ag(I) complexes were found to be diamagnetic, and no *d-d* transitions are expected for such a completely filled d^{10} system, so most likely a tetrahedral geometry is proposed for Ag(I) complex based on FTIR, conductance, and analytical data[4,33,37,38].

ESR spectroscopy measures electron spin directly, in the study of solid-state Cu(II) complex, The geometry and nature of the metal ion's bonding to the nearest neighboring ligand in the paramagnetic

ion are investigated using the ESR method. The octahedral environment around the Cu(II) ion is confirmed by the powder ESR spectrum of the Cu(II) complex at room temperature, which has two g values ($g_{\|}$ = 2.267, $g_{\perp}$ = 2.075).The unpaired electron in axially elongated octahedral complexes occupies the d_{x2_y2} orbital causing $g_{\|} > g_{\perp}$. For that, trend $g_{\|} > g_{\perp} > g_e$ (2.0023) reflected for this complex showing d_{x2_y2} is the ground state with the d^9 copper(II) octahedral geometry around the copper(II) ion in the complex[37]. According to Kivelson and Neiman [37], $g_{\|}$ 2.3 is indicative of covalent characteristics, whereas $g_{\|} > 2.3$ is indicative of ionic characters. This criteria indicates that the Cu(II)-complex under investigation mostly contains covalent metal-ligand bonding. According to Hathaway, the results of ESR research lead to the creation of a new parameter, G, which is defined as $G = (g_{\|} - g_e)/(g_{\perp} - g_e)$, where G is the exchange interaction parameter and g_e is the free electron g-value (2.0023)[38], When G is more than 4, the exchange interaction between copper(II) centres in the solid state is negligible, however when G is less than 4, a large exchange contact is proposed in the solid complex. The estimated G value measured for the copper(II) complex was found to be less than 4, indicating exchange interactions in the solid copper complexes, according to deformed octahedral structure[39].

When contrasting the produced complexes' infrared spectra with those of the free ligand, it was found that the (NH) group is shifted to lower/higher wave number at 3228-3387cm^{-1}, while (C=N) group is shifted to lower wave number at 1655-1690cm^{-1} on complexation[40]. Which confirm that exocyclic (NH) and (C=N) imidazole groups involved in the structural configuration in the complex compounds. A new band seen in the spectra of the generated compounds between 808 and 894 cm^{-1} was also attributable to coordinated water molecules oscillating stretched and out of plane[41]. The thermal gravimetric analysis studies were used to conduct these coordinated water molecules. Additionally, the IR spectra of the metal complexes revealed two additional bands at 524-564cm-1 and 404-487cm-1, which were attributed to the stretching vibrations of the υ(M-O) and υ(M-N) stretching vibration respectively[4].

Table 1. Electronic spectral results of H_2L ligand along with its metal complexes (1-6).

Compound	Absorption bands (nm)						
	Phosphazo ring	π-π*	n-π*	*L-MCT*	*d-d* transition	μeff (B.M)	Geometry
H_2L	**277**	**310**	**-**	**-**	**-**	**-**	**-**
$[(FeCl_3)_2(H_2L)(H_2O)_2]$	**270**	**320**	**363**	**430**	**560**	**6.1**	**Octahedral**
$[(FeSO_4)_2(H_2L)(H_2O)_4]$	**273**	**326**	**369**	**390, 422**	**528, 663, 735**	**4**	**Octahedral**
$[(CuCl_2)_2(H_2L)(H_2O)_4]$	**269**	**324**	**362**	**387, 424**	**573, 667**	**1.7**	**Octahedral**
$[(ZnCl_2)_2(H_2L)(H_2O)_4]$	**272**	**301**	**348**	**d^{10}**			**Octahedral**
$[(CdCl_2)_2(H_2L)(H_2O)_4]$	**274**	**300**	**328**	**d^{10}**			**Octahedral**
$[(AgNO_3)_2(H_2L)(H_2O)_2]$	**268**	**305**	**344**	**d^{10}**			**Tetrahedral**

Table 2. ^{13}C NMR data of H_2L free ligand chemical shift (δ,ppm)

Types of carbon atoms[a]	H_2L	
	Calc.[b]	Obs.
C1 (Methyl carbon)	**21.3**	**20.96**
C2 (o-benzene ring carbon)	**116.2**	**115.9**
C3 (Purine ring carbon)	**119.4**	**121.89**
C4 (m-benzene ring carbon)	**129.8**	**130.43**
C5 (p-benzene ring carbon)	**131.2**	**132.1**
C6 (Imidazole ring carbon)	**138.2**	**137.8**
C7, C8 (benzene ring carbon atoms bound to phospha(V)azo ring nitrogen atoms)	**143.7, 144.8**	**143.0, 147.72**
C9 (Purine ring carbon)	**151.2**	**150**
C10 (pyrimidine ring carbon)	**152.4**	**152.96**

[a] See Scheme.1. for numbering of carbon atoms.
[b] ^{13}C NMR was calculated by Ultra chem.Office[31]

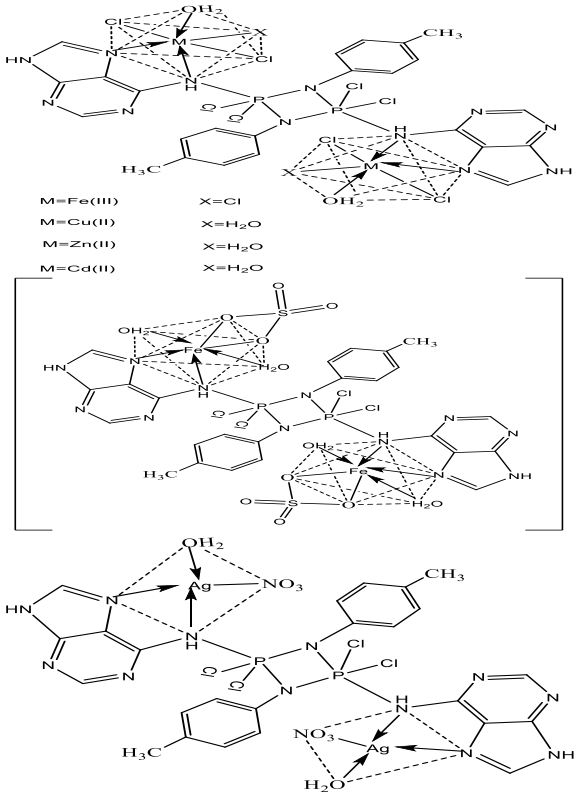

Fig. 2. Suggested structures of metal complexes (1-6)

Within ^{1}H NMR spectra of made diamagnetic complexes (4,5,6), signals observed in δ=6.62-7.28ppm region corresponded to aromatic protons[42]. Also, the peak for (NH) signal in all complexes was shifted slightly down field in range δ=8.86-8.94ppm relative to the free ligand[43]. Other proton signals due to (CH) imidazole and pyrimidine were appeared at 8.48 and 8.49ppm, respectively in all diamagnetic complexes[8]. Signals due to (CH_3) protons appeared at 2.49ppm in all diamagnetic complexes[24]. A new signal due to coordinated water appeared at 3.6-3.9ppm[44].

By means of analysis of powder X-ray diffraction, the crystalline size of the synthesized ligand and its copper complex as a typical example was measured. Crystalline peaks are shown in Figs. 3,4 the powder X-ray form of free ligand and its copper complex by their sharp peaks, which indicate crystalline nature of both. The difference in X-ray between metal complex, more crystalline and its parent ligand is due to the presence of metal ion. Using Debye-equation, Scherrer's it was possible to determine the typical crystalline size of the samples: D=K λ/βCos θ, K is constant equal to 0.94 where θ is the Bragg diffraction angle for the hkl plane, β is the full width half maximum of the characteristic peak and λ is the wavelength of X-ray source utilized, which equal to 1.54 Å[45,46]. From the diffraction peaks the average crystalline size was found to be 15nm for free ligand and 12.8nm for its metal complex.

Table 3: Some chosen quantum chemical parameters for the H_2L free ligand and structural parameters for the B3LYP (bond lengths, bond angles, and dihedral)

Structural parameters	
Bond lengths (Å)	
P_2-N_1= P_4-N_3	**1.665**
P_2-N_3= P_4-N_1	**1.866**
P_2-N_{62}, P_4-N_6	**1.753**
P_2-Cl_8 = P_2-Cl_9 = P_4-Cl_5 = P_4-Cl_7	**2.099**
N_6-H_{63}, N_{62}-H_{64} (Exocyclic NH)	**1.041**
C_{33}-N_{38} = C_{28}-N_{41}	**1.383**
N_{36}-H_{61} = N_{39}-H_{50} (Imidazole NH)	**1.008**
Bond angles °	
P_2-N_1- P_4 = P_2-N_3- P_4	**101.5**
N_1-P_2- N_3 = N_1-P_4- N_3	**78.46**
Cl_8-P_2- Cl_9 = Cl_5-P_4- Cl_7	**111.9**
P_2-N_{62}- C_{29} = P_4-N_6- C_{32}	**131.7**
P_2-N_{62}- H_{64} = P_4-N_6- H_{63}	**115.1**
C_{28}-C_{29}-N_{62} = C_{32}-C_{33}-N_{38}	**132.5**
C_{29}- N_{62}-H_{64} = C_{32}- N_6-H_{63}	**113**
Dihedral angles °	
N_1- P_4-N_3-P_2	**0.00**
N_6- P_4-N_1-N_3	**179.9**
N_{62}- P_2-N_1-N_3	
P_2- N_1-C_{10}-C_{11}	**89.2**
P_2- N_3-C_{18}-C_{19}	**90.5**
Purine ring	**0.00**
Benzene ring	**0.00**
Calculated quantum chemical parameters	
E (a.u)	**-4108**
Dipole moment (Debye)	**6.18**
E_{HOMO} (ev)	**-5.94**
E_{LUMO} (ev)	**-1.63**
ΔE (E_{LUMO} - E_{HOMO}) (ev)	**4.31**
X (ev)	**3.78**
η (ev)	**2.15**
σ (ev)-1	**0.464**
Pi (ev)	**-3.78**
S (ev)-1	**0.232**
ω (ev)	**3.31**

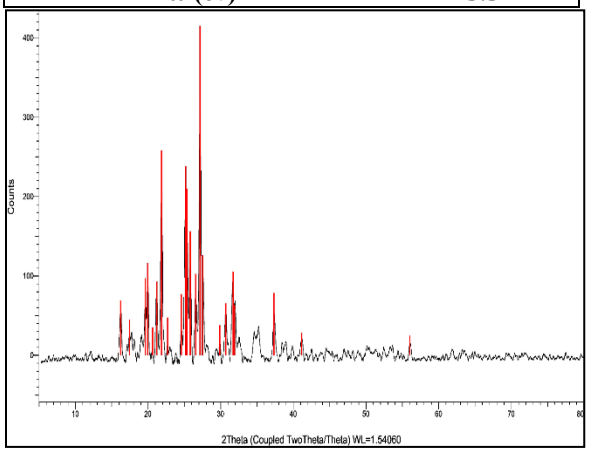

Fig. 3. X-ray powder diffractogram of H_2L free ligand

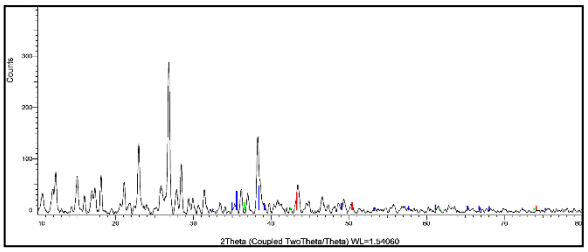

Fig. 4. X-ray powder diffractogram of copper complex (3)

Field emission scanning electron microscopy was used to examine the shape, size, and structure of the silver nano complex (SEM). The SEM micrograph of (H_2L) free ligand and its ordinary and nano silver complexes presented in Fig.5. SEM image showed that the particles shape of free ligand was different than that of the particles of its complexes, due to the presence of the metal ion[47]. The SEM analysis demonstrated that the created nano silver complex, present in nanometers structure with spherical grains shape, which different than the ordinary silver complex in the shape and the size. The average particle size of nano silver complex was 51.9nm. The synthesized nanoparticle size complex may useful in various fields including biological applications[48].

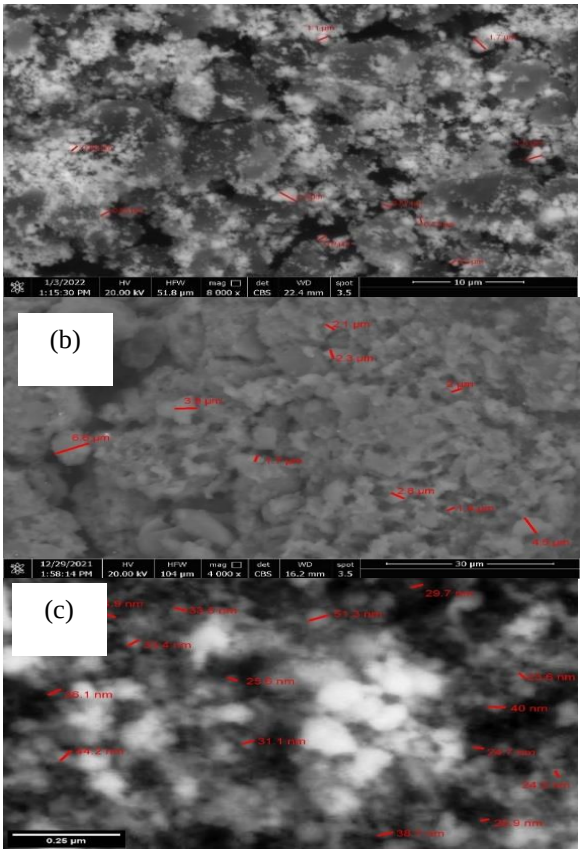

Fig. 5. SEM images of H_2L free ligand (a), its ordinary silver complex (b), and its nano silver complex (c).

Metal complexes' thermogravimetric analysis (TGA) (1,2,3,4,6) were used to provide more information about the structure of the complexes, Thermal investigations were performed to establish whether the water molecules are inside central metal ion's inner coordination sphere (coordinated) or outside it (crystalline), and ultimately to provide a over-all plan for the thermal disintegration of such chelates[49].

Thermal decomposition of Fe(III) complex decomposes in three stages during the course of 102-559°C. The first step occurs in temperature range of 102-125°C which corresponding to the loss of H_2O of coordination, with a found mass loss of 1.72% (calcd. 1.79%); the second step with an estimated mass loss of 59.44% (calcd.59.25%) in the temperature range of 262-340°C corresponds to the loss of H_2O of coordination, $3Cl_2$, $2C_5H_5N_5$ and C_7H_7N. The third step with an anticipated mass loss of 16.01% (calcd. 15.07%) was in the temperature range 514-559°C corresponds to the loss of the organic part $C_7H_7P_2N$ and Fe_2O_3 as a metallic residue. The overall weight loss amounts to77.17 % (calcd. 76.11%).

The Cu(II) complex of the H_2L free ligand, $(CuCl_2)_2(H_2L)$ $(H_2O)_4$, (3) showed four breakdown phases between the temperatures of 43 and 475 ºC on the TGA curve. The initial step takes place between 43-241 ºC, and it corresponds to the loss of $4H_2O$ and an HCN molecule with a mass loss of 9.32% (calculated 9.68%).; the second stage with an estimated mass loss of 12.49% (calculated 12.07%) within the temperature range 241-296ºC corresponds to the decomposition of three molecules of HCl and $_{1/2}N_2$. The third stage with an estimated mass loss of 13.12% (calculated 13.84%) within the temperature range of 296-357ºC corresponds to the loss of one molecule of HCl in addition to losing an organic part, C_7H_7N. The fourth step at the range 357-475ºC with an estimated mas (b) '.25% (calculated 38.16%) attributed to loss ɔrganic parts of the ligand ($C_5H_4N_5P$ & $C_{12}H_6N_4P$) leaving $2CuCl_2$ as a metallic residue. The overall weight loss amounts to 72.3% (calculated73.5%).

Additionally, the fourth decomposition phases of the Cd(II) complex breakdown occur between 249 and 774 °C. Four coordinated molecules of H_2O and two molecules of HCl undergo the first stage of breakdown between 249 and 290 degrees Celsius, with a mass loss of 12.93% (calculated: 12.16%).; The loss of C_7H_7 and one molecule of HCl in the second stage, which has an estimated mass loss of 11.36% (calculated: 11.92%), occurs in the temperature range of 454–470°C. Within the temperature range of 585-679°C, the third stage of breakdown entails the removal of an organic component, namely $C_5H_5N_5$ and C_6H_4, with an estimated weight loss of 18.81% (calculated18.47%). The final stage, which takes place between 773 and

774 ºC, reflects the loss of CH_4, with a found mass loss of 1.42% (calculated at 1.98%)., leaving $C_5H_4N_5$, HCl, P_2N_2 and $2CdCl_2$ as a metallic residue. The total weight decrease is 44.98% (calculated at 44.52%).

The thermal decomposition of the Ag(I) complex $[(AgNO_3)_2(H_2L)(H_2O)_2]$, (6) shows the decomposition pattern as follows: the first step within the temperature range of 218-308ºC, represents the loss of two molecules of coordinated H_2O, two molecules of nitrate and one molecule of HCl, with a found mass loss of 18.7% (calcd. 18.55%). The second step with an estimated mass loss of 8.2% (calcd. 8.61%) within the temperature range 308−408ºC corresponds to the loss of organic part C_7H_7. The third step with an estimated mass loss of 35.1% (calcd. 35.82%) within the temperature range 408-687ºC corresponds to the loss of two organic parts of the ligand $C_5H_4N_5P$ & $C_5H_3N_6P$ and $_{1/2}Cl_2$ leaving C_7H_7N + 2AgCl as a metallic residue. The overall weight amounts to 63.04% (calcd. 62.98%).

By using the Coats-Redfern connection and Horowitze Metzger equation, the thermodynamic activation parameters of complicated decomposition processes are visually evaluated: activation energy (ΔE*), enthalpy (ΔH*), entropy (ΔS*), and Gibbs free energy change (ΔG*)[50]. Excel's complexes program was used to determine the entropy of activation (ΔS*), enthalpy of activation (ΔH*), and the free energy change of activation (ΔG*). Table 4 provides a summary of the data. The complexes' high activation energies reflect their remarkable thermal stability. In the complexes, it is discovered that the entropy of activation (ΔS*) has a negative value, indicating that the breakdown processes happen more slowly than usual. Due to rising TS* values, the (ΔG*) values rise in a way that is adequate for the frequent decomposition stages[51] In all instances, it is discovered that the (ΔH*) are positive values, indicating that the reaction is endothermic. The (ΔH*) values and their sign are depending on the heat of complex formation and the solvent effect[50].

Table 4. H_2L metal complexes' Thermodynamic results (1,3,5,6)

Comp. No.	Complex	Decomposition Temp	Tp/K	R^2		ΔE^* (J mol^{-1})		A (S^{-1})		ΔS^* (K^{-1} mol^{-1})		ΔH^* (J mol^{-1})		ΔG^* (J mol^{-1})	
				HM	CR	HM	CR	HM	CR	HM	CR	HM	CR	HM	CR
(1)	$[(FeCl_3)_2(H_2L)(H_2O)_4]$	102-125	386	0.96	-0.96	1743	257596	$1.26x10^4$	$2x10^{34}$	-226	-804	-1474	254378	86136	565671
		262-340	570	0.99	-0.98	263	56368	$8.28x10^2$	$9.04x10^5$	-200	-258	-4480	51624	109937	199204
		514-559	805	0.95	-0.94	171	55626	$2.52x10^2$	$3.06x10^5$	-187	-246	-6526	48928	144749	247751
(3)	$[(CuCl_2)_2(H_2L)(H_2O)_4]$			HM	CR	HM	CR	HM	CR	HM	CR	HM	CR	HM	CR
		43-241	415	0.96	-0.96	212	30333	$3.09x10^3$	$9.9x10^6$	-214	-381	-3245	26875	85815	143834
		241-296	542	0.93	-0.90	290	75210	$7.2x10^2$	$2.6x10^6$	-199	-268	-4219	70700	104159	216045
		296-357	600	0.94	-0.91	231	72405	$3.7x10^2$	$3.6x10^5$	-193	-250	-4761	67413	111382	217945
		357-475	689	0.88	-0.81	119	43881	$3.2x10^2$	$2.4x10^7$	-190	-284	-5617	38144	125882	234486
(5)	$[(CdCl_2)_2(H_2L)(H_2O)_4]$			HM	CR	HM	CR	HM	CR	HM	CR	HM	CR	HM	CR
		249-290	522	0.98	-0.97	480	136800	$3.8x10^3$	$3.8x10^{12}$	-214	-386	-3886	132455	108010	334358
		454-470	733	0.96	-0.95	476	245348	$6.1x10^2$	$1.6x10^{17}$	-196	-472	-5626	239246	138213	585863
		585-679	898	0.95	-0.91	90	18174	$1.14x10^2$	$6.9x10^6$	-180	-271	-7389	10694	154800	255187
		773-774	1037	0.97	-0.97	1611	$2x10^6$	$4.01x10^3$	$8.6x10^8$	-208	-1823	-7024	$2x10^6$	20983	$4x10^6$
(6)	$[(AgNO_3)_2(H_2L)(H_2O)_2]$			HM	CR	HM	CR	HM	CR	HM	CR	HM	CR	HM	CR
		218-308	536	0.98	-0.97	588	162376	$5.2x10^3$	$6.2x10^{14}$	-216	-428	-3871	157916	112182	387640
		308-408	631	0.99	-0.98	119	36313	$1.4x10^2$	$1.7x10^7$	-185	-282	-5134	31060	111893	209449
		408-687	820	0.92	-0.83	85	43108	$2.3x10^2$	$1.3x10^8$	-187	-297	-6739	36284	146883	280363

2.4. Biological activity

2.4.1. In-vitro cytotoxicity assays

Evaluation the anticancer activity of synthesized H_2L free ligand and its metal complexes on cancer cell lines. The cytotoxicity studies were performed on human being breast carcinoma and human being colorectal carcinoma cell lines (MCF-7 & HCT-116) and IC_{50} values were detected using doxorubicin as a standard are listed in Table 5 and shown in Figs. 6,7,8.

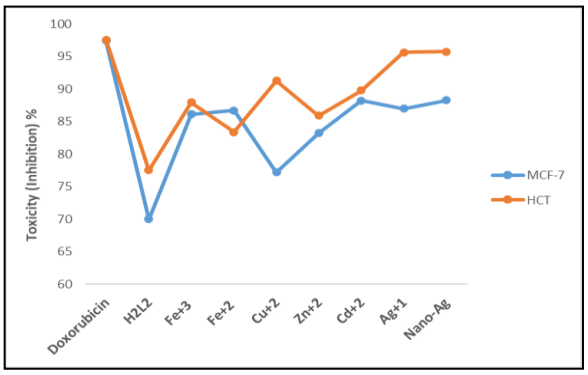

Fig.6. Antitumor activity of H_2L ligand and its complexes (1-7) against MCF-7 and HCT-116 cell lines.

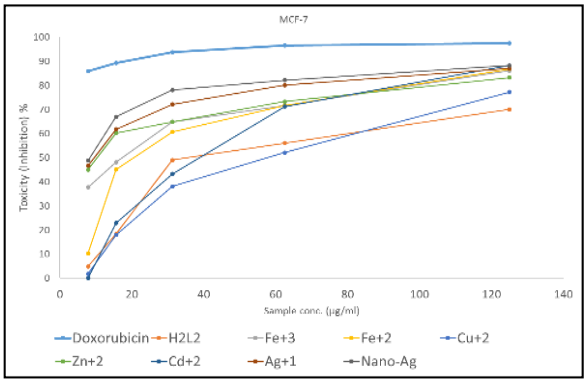

Fig.7. Drug cytotoxicity for H_2L free ligand along with its metal complexes (1-7) against MCF-7 and HCT-116 cell lines at different concentrations.

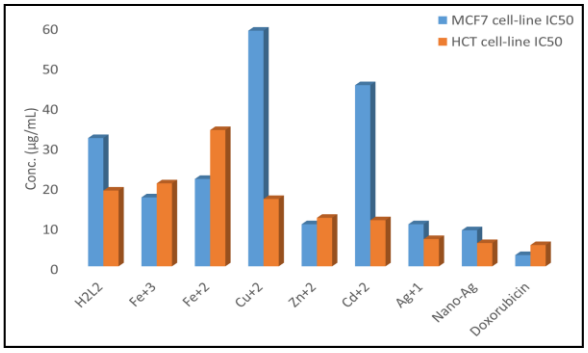

Fig.8. IC_{50} for H_2L free ligand and its metal complexes (1-7) against MCF-7 and HCT-116 cell lines.

Table 5. Antitumor activity and (IC_{50}µM) of H_2L along with its metal complexes (1-7).

Sample	Inhibition %		(IC_{50} µM)	
	MCF 7 cell line	HCT-116 cell line	MCF 7 cell line	HCT-116 cell line
H_2L	70.02	77.54	32.0	18.9
(1) $[(FeCl_3)_2(H_2L)(H_2O)_2]$	86.11	87.98	17.2	20.7
(2) $[(FeSO_4)_2(H_2L)(H_2O)_4]$	86.75	83.38	21.8	34.0
(3) $(CuCl_2)_2(H_2L)(H_2O)_4]$	77.23	91.32	58.8	16.8
(4) $[(ZnCl_2)_2(H_2L)(H_2O)_4]$	83.22	85.92	10.5	12.1
(5) $[(CdCl_2)_2(H_2L)(H_2O)_4]$	88.23	89.81	45.2	11.5
(6) $[(AgNO_3)_2(H_2L)(H_2O)_2]$	86.97	95.64	10.5	6.8
(7) Nano-Ag complex	88.28	95.74	9.0	5.8
Doxorubicin	97.43	97.57	4.3	5.3

(IC_{50} µM): 1-10 (extraordinarily strong), 11-20 (strong), 21-50 (moderate), 51-100 (non-cytotoxic).

H_2L free ligand gave a remarkable activity against two both cell lines with inhibition values equal to 70.02 and 77.54%, IC_{50}= 32.0 and 18.9 µM for MCF-7 and HCT-116 cell lines, respectively. Nano silver complex gave the best IC_{50}= 9.0 and 5.8 µM with perfect inhibition values equal to 88.28, 95.74% for MCF-7 and HCT-116 cell lines, respectively.

The order of anticancer activities according to IC_{50}:

Cell line	Order of anticancer activities
MCF-7 cell line	**Nano Ag > Ag(I) = Zn(II) > Fe(III) > Fe(II) > H_2L free ligand > Cd(II) > Cu(II)**
HCT-116 cell line	**Nano Ag > Ag(I) > Cd(II) > Zn(II) > Cu(II) > H_2L free ligand > Fe(III) > Fe(II)**

These results recommended as new results of promising antitumor drugs for MCF-7 and HCT-116 cell lines.

2.4.2. Antimicrobial

The primary goal of making any antibacterial agent is to suppress the microorganism without having any negative effects on patients[50].

The antimicrobial activity of the parent ligand H_2L and its prepared metal complexes were screened against microorganism, Gram positive (+ve) bacteria; *Bacillus pumilis (MTCC – 2296) and*

Streptococcus faecalis (MTCC – 0459), Gram negative (-ve) bacteria *Escherichia coli (ATCC-25922)* and *Enterobacter cloacae (ATCC 23355)*, yeast; *Candida albicans (ATCC 10231)* and fungi; *Aspergillus niger (MTCC-1881)* to assess their potential antimicrobial agents

According to the agar plate diffusion method, the antibacterial ability of recently synthesized compounds was examined against the tested microorganisms and expressed as the width of the inhibitory zones[52].

The minimum inhibitory concentration (MIC) and the effects of the free ligand and its metal complexes on bacterial, yeast, and fungal species were noted in Table 6, the results lead to the following conclusions:

H_2L free ligand displays high to intermediate activity with MIC range 1.95-62.5µg/ml against Gram positive (+ve), Gram negative (-ve) strains of bacteria, yeasts, and fungi. All metal complexes showed particularly good readings against all microorganism types, while silver complex show better results in nano structure towards the tested microorganisms. In Table 6 and Figs. 9, 10, the newly synthesized compounds' effects on Gram positive (+ve) and Gram negative (-ve) bacteria, yeasts, and fungi species, as well as their MIC values, are shown.

The metal complexes of the H_2L ligand's action are listed below.:

Organism	Orders of the activity
Bacillus pumilis (MTCC – 2296)	**Nano silver complex > Fe(II) =Ag(I) >Fe(III) >Cd(II) >Cu(II) = Zn(II)**
Streptococcus faecalis (MTCC – 0459)	**Cd(II) >Nano silver complex = Zn(II) >Fe(II) > Fe(III) >Ag(I) > Cu(II)**
Escherichia coli (ATCC 25922)	**Fe(II) >Zn(II) > Fe(III) >Cd(II)> Nano silver complex =Cu(II) > Ag(I)**
Enterobacter cloacae (ATCC 23355)	**Fe(III)>Fe(II) > Nano silver complex> Cd(II) > Zn(II) > Ag(I) > Cu(II)**
***Candida albicans* (ATCC-10231)**	**Cu(II) > Zn(II) > Nano silver complex =Cd(II) > Ag(I) > Fe(II) > Fe(III)**
Aspergillus niger (MTCC -1881)	**Zn(II) > Nano silver complex > Fe(II) = Ag(I) > Cd(II) > Fe(III) =Cu(II)**

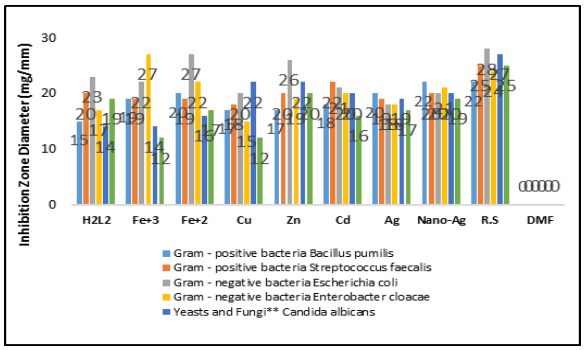

Fig.9: Antibacterial Activity of H_2L free ligand along with its metal complexes (1-7).

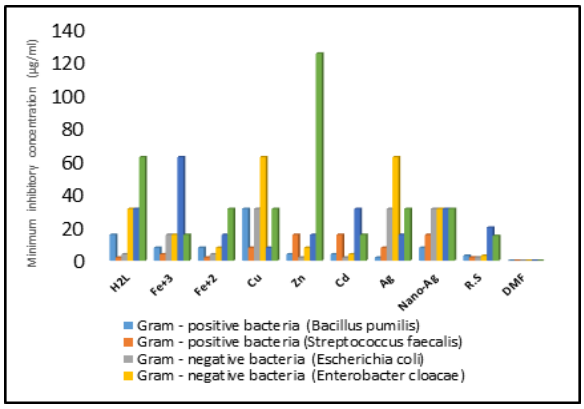

Fig.10: H_2L along with its metal complexes' MIC (1-7)

Table 6. H_2L ligand and its complexes' Antimicrobial activity (1-7).

	Mean* of zone diameter, nearest whole mm.											
Organism / Sample	Gram-positive bacteria				Gram-negative bacteria				Yeasts and Fungi**			
	***B. pumilis* (MTCC – 2296)**		***S. faecalis* (MTCC – 0459)**		***E. coli* (ATCC - 25922)**		**E. cloacae (ATCC 23355)**		***C. albicans* (ATCC 10231)**		***A. niger* (MTCC -1881)**	
	IZ	**MIC**	**IZ**	**MIC**	**IZ**	**MIC**	**IZ**	**MIC**	**IZ**	**MIC**	**IZ**	**MIC**
H_2L	**15**	**15.63**	**20**	**1.95**	**23**	**3.91**	**17**	**31.3**	**14**	**31.3**	**19**	**62.5**
(1) $[(FeCl_3)_2(H_2L)(H_2O)_2]$	**19**	**7.81**	**19**	**3.91**	**22**	**15.63**	**27**	**15.63**	**14**	**62.5**	**12**	**15.63**
(2) $[(FeSO_4)_2(H_2L)(H_2O)_4]$	**20**	**7.81**	**19**	**1.95**	**27**	**3.91**	**22**	**7.81**	**16**	**15.63**	**17**	**31.3**
(3) $[(CuCl_2)_2(H_2L)(H_2O)_4]$	**17**	**31.3**	**18**	**7.81**	**20**	**31.3**	**15**	**62.5**	**22**	**7.81**	**12**	**31.3**
(4) $[(ZnCl_2)_2(H_2L)(H_2O)_4]$	**17**	**3.91**	**20**	**15.63**	**26**	**1.95**	**19**	**7.81**	**22**	**15.63**	**20**	**125**
(5) $[(CdCl_2)_2(H_2L)(H_2O)_4]$	**18**	**3.91**	**22**	**15.63**	**21**	**1.95**	**20**	**3.91**	**20**	**31.3**	**16**	**15.63**
(6) $[(AgNO_3)_2(H_2L)(H_2O)_2]$	**20**	**1.95**	**19**	**7.81**	**18**	**31.3**	**18**	**62.5**	**19**	**15.6**	**17**	**31.3**
(7) Nano-silver complex	**22**	**7.81**	**20**	**15.6**	**20**	**31.3**	**21**	**31.3**	**20**	**31.3**	**19**	**31.3**
R.S**	**22**	**≤ 3**	**25**	**≤ 2**	**28**	**≤ 2**	**24**	**≤3**	**27**	**≤20**	**25**	**≤15**

*Utilizing the diffusion agar method, the test was conducted. Inhibition values ≤ 10 (less active). Inhibition values ≤15 (moderately active). Inhibition values > 20 (highly active). Not active = 0.

**The antibiotic Penicillin G was used as the standard reference in the case of Gram-positive bacteria, Ciprofloxacin was used as the standard reference in the case of Gram-negative bacteria, and In the case of yeasts and fungi, ketoconazole served as the standard reference.

3. Conclusion

In this work, we have synthesized and characterized a cyclodiphosph(V)azane derivative-based 9H-purin-6-amine and its metal complexes. The data showed that the free ligand was coordinated with metal ions through exocyclic-NH and pyrimidine-N. Complexes' excellent thermal stability was validated by their thermal degradation stages. Additionally, every metal complex is more active than the equivalent free ligand, according to antibacterial screening results. Comparing the antitumor data of all complexes, we found that nanosilver complex showed the best IC_{50} value equal to 90 and 58µM for two cell lines (MCF-7 and HCT-116); respectively with excellent anticancer activity.

4. Conflicts of interest

There are no conflicts to declare.

5. Formatting of funding sources

No funding sources available to declare.

6. Acknowledgment

We are thankful to Cairo University's Micro Analytical Center, Giza, Egypt for helping in analysis process.

7. References

1. P. Kommana and K. C. Kumara Swamy; Synthesis and Structural Characterization of a New Class of Macrocycles Based on a Cyclodiphosphazane Skeleton, *Inorganic Chemistry*, **39**, (4384-4385) **2000**. https://doi.org/10.1021/ic000359o
2. K.P.Kumar, M.Chakravarty and K.C.K.Swamy; Synthesis and Structures of New Oxidation/ Cycloaddition Products of λ3-Cyclodiphosphazanes, *Z. Anorg Allg. Chem.*, **630**, (2063-2070) **2004**. https://doi.org/10.1002/zaac.200400275
3. A. M. A. Alaghaz; Studies of Some New Aminocyclodiphosphazane Complexes of Co(II), Ni(II), and Cu(II), *Phosphorus, Sulfur, and Silicon*, **183**, (2476–2489) **2008**. https://doi.org/10.1080/10426500801964077
4. Gehad G. Mohamed; New Cyclodiphosph(V)azane Complexes of Fe(III), Co(II), Ni(II), Cu(II), Zn(II), and UO_2 (II): Preparation, Characterization, and Biological Activity Studies, *Phosphorus, Sulfur, and Silicon*, **180**, (1569–1586) **2005**. https://doi.org/10.1080/104265090884238
5. T. Roth, H. Wadepohl, D. S. Wright and L. H. Gade; Chiral Ditopic Cyclophosphazane (CycloP) Ligands: Synthesis, Coordination Chemistry, and Application in Asymmetric Catalysis, *Chemistry-A European Journal*, **19**, (13823-13837) **2013**. https://doi.org/10.1002/chem.201302327
6. Mingsheng Liu, Shuo Huang, Guangxian Zhang and Fengxiu Zhang; Synthesis of P–N–Si synergistic flame retardant based on a cyclodiphosphazane derivative for use on cotton fabric, *Cellulose*, **26**, (7553–7567) **2019**. https://doi.org/10.1007/s10570-019-02608-5
7. Abdel-Nasser M. A. Alaghaz and Sharah A. A. Aldulmani; Preparation, Structural characterization and DNA binding/cleavage affinity of new bioactive nano-sized metal (II/IV) complexes with oxazon-Schiff's base ligand, *Journal of the Chinese Chemical Society*, (1–11) **2019**. https://doi.org/10.1002/aoc.5135
8. Tarek A. Mohamed, Wajdi M. Zoghaib, Ibrahim A. Shaaban, Rabei S. Farag and Abd Elnasser M.A. Alajhaz; Infrared, ^{1}H and ^{13}C NMR spectra, structural charcterization and DFT calculations of novel adenine-cyclodiphosp(V)azane derivatives, *Spectrochimica Acta*, **83,** (304– 313) **2011**. https://doi.org/10.1016/j.saa.2011.08.035
9. Rahul B. Aochar, R. G. Mahale, and Ravindra S. Dhivare; Synthesis, Physicochemical, Morphological, and Antimicrobial Study of Schiff-Base Ligands Metal Complexes, *Journal of Research in Pharmaceutical Science*, **8,** 2, (1-6) **2022**. https://www.questjournals.org/jrps/v8-i2.html
10. M. S. Masoud, A. El-Merghany, A. M. Ramadan and M. Y. Abd El-Kaway; Thermal studies of some purine compounds and their metal complexes, *Journal of Thermal Analysis and Calorimetry*, **101**, (839–847) **2010**. https://doi.org/10.1007/s10973-010-0722-z
11. Teresa F. Mastropietro, Donatella Armentano, Ettore Grisolia, Claudia Zanchini, Francesc Lloret and Miguel Julveb and Giovanni De Munno; Guanine-containing copper(ii) complexes: synthesis, X-ray structures and magnetic properties, *Dalton Transactions The Royal Society of Chemistry*, (514–520) **2008**. https://doi.org/10.1039/B713960H
12. Hamad M. I. Hasan, Aaza I. Yahiya, Safaa S. Hassan and Mabrouk M. Salama; Biological Study of Transition Metal Complexes with Adenine Ligand, *Proceedings*, **41**, 77, **2019**. https://doi.org/10.3390/ecsoc-23-06601
13. Thomas Hielscher; Ultrasonic Production of Nano-Size Dispersions and Emulsions, *European Nano Systems*, Paris, France, (14-16) **2005**. https://doi.org/10.48550/arXiv.0708.1831
14. J. Bassett, R. C. Denney, G. H. Jeffery, and J. Mendham; Vogel's Textbook of Quantitative

Inorganic Analysis, 4th ed.; England: Longman, pp 130-131, **1978**.
15. A. Gohn. ESR and Elementary Particle Applications, New York: Wiley, **1986**.
16. E. Normaya, M. Hamdan, M.N. Ahmed, Y. F. Abdul Aziz and K. Bulat; DFT/TD-DFT study on development and optimization of 1-anilino-3-phenyliminourea as a colorimetric chemosensor for Hg^{2+} recognition in aqueous medium, *Journal of Molecular Structure*, **1194**, (187-203) **2020**. https://doi.org/10.1016/j.molstruc.2020.127699
17. J. Rodriguez-Tudela, F. Barchiesi, J. Bille and E. Chryssanthou; Method for the determination of minimum inhibitory concentration (MIC) by broth dilution of fermentative yeasts, *Clinical Microbiology, and Infection*, **9**, (1–8) **2003**. https://doi.org/10.1046/j.1469-0691.2003.00789.x
18. I.M. Abd-Ellah, Y. Al-Shaibi, A.A. Ba-Issa, and M.S. El-Hammadi; spectroscopic study on the electron delocalization within the phosphazo ring, *Phosphorous, Sulfur, and Silicon*, **139**, (29-43) **1998**. https://doi.org/10.1080/10426509808035675
19. K. Salib, A.A Saleh, S. Abu El-Wafa, and H.F.O. El-Shafiy; Preparation and Characterization of Novel Asymmetrical Schiff-Base Ligands Derived from 2-methyl-7-formyl-8-hydroxyquinoline and their Metal Complexes, *Journal of Coordination Chemistry*, **56**, (283–298) **2003**. https://doi.org/10.1080/00958970310000690 21
20. C.M. Sharaby, "Studies of the Chemical Reactivity of Some Compounds Containing Amino Group", Ph.D. Thesis, *Al–Azhar University (Girls)*, (58–63) **1992**.
21. Rania H. Taha, ph.D. Thesis, Faculty of Science, *Al-Azhar University (Girls)*, Cairo, Egypt, **2014**.
22. Mamdouh S. Masouda, Amina A. Soayed and Alaa E. Ali; Complexing properties of nucleic-acid constituents adenine and guanine complexes, *Spectrochimica Acta Part A*, **60**, (1907–1915) **2004**. https://doi.org/10.1016/j.saa.2003.09.025
23. R. M. Silverstein, F. X. Webster, D, Kiemle, Spectrometric Identification of Organic compounds, New York: John Wiley, **2004**.
24. C.M. Sharaby; Synthesis, spectroscopic, thermal and antimicrobial studies of some novel metal complexes of Schiff base derived from [N1-(4-methoxy-1,2,5-thiadiazol-3-yl)sulfanilamide] and 2-thiophene carboxaldehyde, *Spectrochemica (A)*, **66**, (1271− 1278) **2007**. https://doi.org/10.1016/j.saa.2006.05.030
25. Khadija E. Saadon, Nadia M. H. Taha, N. A. Mahmoud, Gameel A. M. Elhagali and Ahmed Ragab; *Journal of the Iranian Chemical Society*, published online 12 May **2022**.
26. Carmen M. Sharaby; Studies of Some New Cyclodiphosphazane Complexes of Fe(III), Fe(II), Co(II), Ni(II), Cu(II), Zn(II) and Cd(II), *Metal-Organic and Nano-Metal Chemistry*, **35**, (133–142) **2005**. https://doi.org/10.1081/SIM-200035687
27. Khadija E. Saadon, Nadia M. H. Taha, N. A. Mahmoud, Gameel A. M. Elhagali and Ahmed Ragab; Synthesis, characterization, and in vitro antibacterial activity of some new pyridinone and pyrazole derivatives with some in silico ADME and molecular modeling study, *Journal of the Iranian Chemical Society*, **19**, (3899-3917) **2022**. https://doi.org/10.1007/s13738-022-02575-y
28. Rahila Huma, Tariq Mahmud, Sana Javaid Awan, Muhammad Ashraf, Shafi Ullah Khan d, Humaira Rasheed, Syeda Marium Hasany and Amna Yousaf; Thermal and spectroscopic studies of some metal complexes with a new enaminone ligand 3-chloro-4-((4-methoxyphenyl)amino)pent-3-en-2-one and their investigation as anti-urease and cytotoxic potential drugs, *Arabian Journal of Chemistry*, **15**, (103640) **2022**. https://doi.org/10.1016/j.arabjc.2021.103640
29. E. Normaya, M. Hamdan, M.N. Ahmed, Y. F. Abdul Aziz and K. Bulat; DFT/TD-DFT study on development and optimization of 1-anilino-3-phenyliminourea as a colorimetric chemosensor for Hg^{2+} recognition in aqueous medium, *Journal of Molecular Structure*, **1194**, (187-203) **2020**. https://doi.org/10.1016/j.molstruc.2020.127699
30. Ahmed M. Ramadan, Hoda A. Bayoumi, and Rehab M. I. Elsamra; Synthesis, characterization, biological evaluation, and molecular docking approach of nickel (II) complexes containing O, N-donor chelation pattern of sulfonamide-based Schiff bases, *Applied Organometallic Chemistry*, **6412**, (1-15) **2021**. https://doi.org/10.1002/aoc.6412
31. Sachin B. Pandya, Urmila H. Patel, Kaushik P. Chaudhary, Bhavesh N. Socha, Nikita J. Patel and Bhupesh S. Bhatt; DNA interaction, cytotoxicity and molecular structure of cobalt complex of 4-amino-N-(6-chloropyridazin-3-yl)benzene sulfonamide in the presence of secondary ligand pyridine, *Applied Organometallic Chemistry*, **33**:e5235, (1-14) **2019**. https://doi.org/10.1002/aoc.5235

32. Chem. Office Ultra, 10th ed., Molecular Modelling and Analysis, Cambridge, **2006**.
33. Abdel-Nasser M. A. Alaghaz and Sharah A. A. Aldulmani; Novel 13,14-dimethyl-5,8-dioxa-2,11,13,14-tetraaza-1,12-diphosphabicyclo [10.1.1] tetradecane 1,12-dioxide ligand and its Ni(II), Co(II), and Cu(II) complexes: Synthesis, characterization, antimicrobial, DNA cleavage, and computational studies, *Journal of the Chinese Chemical Society*, **66,** (1300-1310) **2019**. https://doi.org/10.1002/jccs.201800464
34. Ikechukwu P. Ejidike, Mercy O. Bamigboye and Hadley S. Clayton; Spectral, in vitro antiradical and antimicrobial assessment of copper complexes containing tridentate Schiff base derived from dihydroxybenzene functionality with diaminoethylene bridge, *Spectroscopy Letters*, **54,** 3, (212-230) **2021**. https://doi.org/10.1080/00387010.2021.1893191
35. Carmen M. Sharaby; Preparation, characterization and biological activity of Fe(III), Fe(II), Co(II), Ni(II), Cu(II), Zn(II), Cd(II) and UO2(II) complexes of new cyclodiphosph(V)azane of sulfaguanidine, *Spectrochimica Acta Part A*, **62**, (326–334) **2005**. https://doi.org/10.1016/j.saa.2004.12.047
36. Walaa H. Mahmoud, Gehad G. Mohamed and Omnia Y. El-Sayed; Coordination compounds of some transition metal ions with new Schiff base ligand derived from dibenzoyl methane. Structural characterization, thermal behavior, molecular structure, antimicrobial, anticancer activity and molecular docking studies, *Applied Organometallic Chemistry*, **e4051**, (1–21) **2017**. https://doi.org/10.1002/aoc.4051
37. Abdou Saad El-Tabl, Moshira Mohamed Abd-El Wahed, Manar M. Abd-ELwareth and Shaimaa Mohamed Faheem; Nano metal complexes in cancer therapy, preparation, spectroscopic, characterization and anti-breast cancer activity of new metal complexes of alanine Schiff-base, *Egyptian Journal of Chemistry*, **64**, 6, (3131–3152) **2020**. https://doi.org/10.21608/EJCHEM.2021.52415.3082
38. M. Aljahdali and Ahmed A. EL-Sherif; Synthesis, characterization, molecular modeling and biological activity of mixed ligand complexes of Cu(II), Ni(II) and Co(II) based on 1,10-phenanthroline and novel thiosemicarbazone, *Inorganica Chimica Acta*, **407**, (58–68) **2013**. https://doi.org/10.1016/j.ica.2013.06.040
39. Mostafa Y. Nassar, Hisham M. Aly, Moustafa E. Moustafa and Ehab A. Abdelrahman; Synthesis, Characterization and Biological Activity of New 3-substitued-4-amino-5-hydrazino-1,2,4-triazole Schiff Bases and Their Cu(II) Complexes: A New Approach to CuO Nanoparticles for Photocatalytic Degradation of Methylene Blue Dye, *Journal of Inorganic and Organometallic Polymers and Materials*, **27,** (13) **2017**. https://doi.org/10.1007/s10904-017-0569-x
40. Hassan H. Hammud, Georges Nemer, Walid Sawma, Jhonny Touma, Pascale Barnabe, Yolla Bou-Mouglabey, Amer Ghannoum and Jida El-Hajjar; Copper–adenine complex, a compound, with multi-biochemical targets and potential anti-cancer effect, *Chemico-Biological Interactions*, **173**, 2, (84–96) **2008**. https://doi.org/10.1016/j.cbi.2008.03.005
41. Abdel-Nasser M. A. Alaghaz and Salwa A. H. Elbohy; New Tetrachlorocyclodiphosph(V)azane Complexes of Co(II), Ni(II), and Cu(II): Preparation, Characterization, Solid State Electrical Conductivity, and Biological Activity Studies, *Phosphorus, Sulfur, and Silicon*, **183**, (2000–2019) **2008**. https://doi.org/10.1080/10426500701839858
42. Carmen M. Sharaby, Mona F. Amine and Asmaa A. Hamed; Synthesis, structure characterization and biological activity of selected metal complexes of sulfonamide Schiff base as a primary ligand and some mixed ligand complexes with glycine as a secondary ligand, *Journal of Molecular Structure*, **1134**, (208-216) **2017**. https://doi.org/10.1016/j.molstruc.2016.12.070
43. N. Nanjundan, R. Narayanasamy, S. Geib, K. Velmurugan, R. Nandhakumar, M. Dakshinamoorthi Balakumaran and P. T. Kalaichelvan; Distorted tetrahedral bis-(N,S) bidentate Schiff base complexes of Ni(II), Cu(II) and Zn(II): Synthesis, characterization and biological studies, *Polyhedron*, **110**, (203-220) **2016**. https://doi.org/10.1016/j.poly.2016.02.049
44. N.M. Hosny, N. Nawar, S.I. Mostafa and M.M. Mostafa; Spectral characterization of metal complexes derived from glycine (Gly) and 2-acetylpyridine (2-APy), *Journal of Molecular Structure*, **1001**, (62–67) **2011**. https://doi.org/10.1016/j.molstruc.2011.06.019
45. N. Nageswara Rao, E. Kishan, K. Gopichand, R. Nagaraju, AbdulMajeed Ganai and P. Venkateswar Rao; Design, synthesis, spectral characterization, DNA binding, photo cleavage and antibacterial studies of transition

metal complexes of benzothiazole Schiff base, *Chemical Data Collections*, **27**, (100368) **2020**. https://doi.org/10.1016/j.cdc.2020.100368

46. G. Y. Nagesh and B. H. M. Mruthyunjayaswamy; Synthesis, characterization and biological relevance of some metal (II) complexes with oxygen, nitrogen and oxygen (ONO) donor Schiff base ligand derived from thiazole and 2-hydroxy-1-naphthaldehyde, *Journal of Molecular Structure*, **1085**, (198-206) **2015**. https://doi.org/10.1016/j.molstruc.2014.12.058
47. Walaa H. Mahmoud, Reem G. Deghadi and G. Mohamed; Metal complexes of novel Schiff base derived from iron sandwiched organometallic and 4-nitro-1,2-phenylenediamine: Synthesis, characterization, DFT studies, antimicrobial activities and molecular docking, *Applied Organometallic Chemistry*, **e4289**, (1-22) **2018**. https://doi.org/10.1002/aoc.4289
48. A. M. A. Alaghaz, M. E. Zayed and S. A. Alharbi; Synthesis, spectral characterization, molecular modeling and antimicrobial studies of tridentate azo-dye Schiff base metal complexes, *Journal of Molecular Structure*, **1084**, (36-45) **2015**. https://doi.org/10.1016/j.molstruc.2014.12.013
49. G.G. Mohamed, M.M. Omar and A.M. Hindy; Metal Complexes of Schiff Bases: Preparation, Characterization, and Biological Activity, *Turkish Journal of Chemistry*, **30**, (361-382) **2006**. https://journals.tubitak.gov.tr/chem/vol30/iss3/11
50. F. A. Saad and A. M. Khedr; Greener solid state synthesis of nano-sized mono and homo bi-nuclear Ni(II), Co(II), Mn(II), Hg(II), Cd(II) and Zn(II) complexes with new sulfa ligand as a potential antitumour and antimicrobial agents, *Journal of Molecular Liquids*, **231**, (572-579) **2017**. https://doi.org/10.1016/j.molliq.2017.02.046
51. M.M.H. Khalil, E.H. Ismail, G.G. Mohamed, E.M. Zayed and A. Badr; Synthesis and characterization of a novel schiff base metal complexes and their application in determination of iron in different types of natural water, *Open Journal of Inorganic Chemistry*, **2**, (13-21) **2012**. https://doi.org/10.4236/ojic.2012.22003
52. Marwa A.M.Sh. El-Sharief, Samir Y. Abbas, Medhat A. Zahran, Yehia A. Mohamed, Ahmed Ragab and Yousry A. Ammar; New 1,3-diaryl-5-thioxo-imidazolidin-2,4-dione derivatives: synthesis, reactions and evaluation of antibacterial and antifungal activities, *Z. Naturforsch*., **71**, 8, (875–881) **2016**. https://doi.org/10.1515/znb-2016-0054